ISSN 1063-780X, Plasma Physics Reports, 2018, Vol. 44, No. 2, pp. 289–298. © Pleiades Publishing, Ltd., 2018.
Original Russian Text © I.N. Kartashov, M.V. Kuzelev, P.S. Strelkov, V.P. Tarakanov, 2018, published in Fizika Plazmy, 2018, Vol. 44, No. 2, pp. 250–260.

PLASMA ELECTRONICS

Influence of Plasma Unsteadiness on the Spectrum and Shape of Microwave Pulses in a Plasma Relativistic Microwave Amplifier

I. N. Kartashov[a, *], M. V. Kuzelev[a, **], P. S. Strelkov[b], and V. P. Tarakanov[c, d]

[a] *Faculty of Physics, Moscow State University, Moscow, 119991 Russia*
[b] *Prokhorov General Physics Institute, Russian Academy of Sciences, Moscow, 119991 Russia*
[c] *Joint Institute for High Temperatures, Russian Academy of Sciences, Moscow, 125412 Russia*
[d] *National Research Nuclear University "MEPhI", Moscow, 115409 Russia*
**e-mail: igorkartashov@mail.ru*
***e-mail: kuzelev@mail.ru*

Received May 17, 2017; in final form, June 22, 2017

Abstract—Dependence of the shape of a microwave pulse in a plasma relativistic microwave amplifier (PRMA) on the initial plasma electron density in the system is detected experimentally. Depending on the plasma density, fast disruption of amplification, stable operation of the amplifier during the relativistic electron beam (REB) pulse, and its delayed actuation can take place. A reduction in the output signal frequency relative to the input frequency is observed experimentally. The change in the shape of the microwave signal and the reduction in its frequency are explained by a decrease in the plasma density in the system. The dynamics of the plasma density during the REB pulse is determined qualitatively from the experimental data by using the linear theory of a PRMA with a thin-wall hollow electron beam. The processes in a PRMA are analyzed by means of the KARAT particle-in-cell code. It is shown that REB injection is accompanied by an increase in the mean energy of plasma electrons and a significant decrease in their density.

DOI: 10.1134/S1063780X1802006X

1. INTRODUCTION

In an experiment with a plasma relativistic microwave amplifier (PRMA), an unusual result was obtained: the maximum microwave power was observed at the end of the relativistic electron beam (REB) pulse, 200–300 ns after the front of the voltage pulse at the accelerator cathode. As a rule, relativistic vacuum microwave electronics encounters problems with the generation of long microwave pulses (longer than 100 ns). In the S band ($\lambda_0 = 7.5–15$ cm), a power higher than 100 MW was achieved only in microwave pulses shorter than 150 ns [1]. Such limitation was observed in many works, and the problem of pulse shortening has been the subject of a number of international meetings (see, e.g., [2]). Studies aimed at finding reasons for the limitation of the microwave pulse duration were carried out at the Institute of High-Current Electronics [3], Prokhorov General Physics Institute [4], and Institute of Applied Physics [5] of the Russian Academy of Sciences and other laboratories. A review of results of these studies can be found in [1]. Several mechanisms for this phenomenon related to the appearance of plasma in different parts of the microwave generator were revealed. At high magnitudes of the electric field, plasma appeared on the walls of the corrugated waveguide of the microwave generator, which led to a change in the properties of the electrodynamic structure and disruption of generation. There was also another reason for the appearance of plasma on the walls of the corrugated waveguide: the plasma generated at the cathode of the explosive emission diode expanded in the radial direction, due to which the diameter of the electron beam increased and the beam electrons began to hit the walls of the microwave generator. Finally, it was found that the formation of collector plasma can also affect the duration of the microwave pulse. In this paper, we attempt to explain the observed shape of the PRMA output power with a maximum at the end of the microwave pulse.

In [6], it was found that the radius of the electron beam decreased with time, and we attempted to use this fact to explain the observed variation in the microwave power during the REB pulse. In the experiment [6], the voltage pulse at the accelerator cathode had a complicated shape. After the voltage reached its maximum value at $t = 100$ ns, it dropped by 20% and, 100 ns later, reached a plateau. Since the electron energy during the first 200 ns depended on time, it was

difficult to interpret the change in the REB structure and the process of amplification of the plasma wave in this stage. Therefore, in 2015, we modified the shape of the voltage pulse. Now, the maximum voltage is reached just after the front of the pulse and remains almost unchanged (to within 3%) for 300–350 ns. The phenomenon of a decrease in the beam radius with time is still preserved. In [7], a numerical model adequately describing the observed decrease in the REB radius was developed. This made it possible to calculate the time evolution of the REB parameters. It was found that the main REB parameters, such as the beam radius and the spreads in the electron energy and the electron longitudinal momentum, vary weakly in time and, therefore, their time evolution cannot lead to a change in the microwave power during the REB pulse. Analysis of the experimentally observed variation in the output frequency during the REB pulse led to an idea that the observed shape of the microwave pulse is explained by a decrease in the plasma density during the REB.

2. MEASUREMENTS OF THE PARAMETERS OF MICROWAVE PULSES

The description of the PRMA used in these experiments can be found in [6]. The rise time of the voltage pulse accelerating the electron beam is 180 ns, and the duration of the voltage plateau is 300–350 ns. The electron velocity at the voltage plateau is constant to within 1%, and the electron energy is 500 keV. The electron beam current is 2 kA. A microwave pulse from a magnetron with a power of about 50 kW is fed to the input of the amplifier, and, at its output, a microwave pulse with a power of higher than 100 MW and duration of 200–400 ns is detected. The amplifier was tested at three frequencies: 2.40, 2.71, and 3.10 GHz. The stability of the magnetron frequency was better than 1 MHz. In this paper, we present experimental data obtained only for the input frequency of 2.71 GHz; however, all the characteristic features discussed below were also observed at the other two frequencies. Before each REB current pulse, plasma with a known electron density n_p (in relative units) was prepared [8]. Measurements of the absolute electron density in the given system are difficult to perform. According to the theory of beam–plasma interaction and experimental data, the absolute value of n_p was in the range of $(1–2)\times10^{12}$ cm^{-3}.

Figure 1 shows waveforms of the microwave signal at the output of the PRMA for different values of the initial electron density. Along with the amplified harmonic signal, these waveforms also contain amplified electron beam noise. Of course, the frequency spectrum of this noise differs from the spectrum of the harmonic signal. Signals shown in Fig. 1 were processed by a ±15-MHz bandpass filter. The measured signal is shown in black, while the signal in the frequency band of 2710 ± 15 MHz is shown in gray. The change in the shape of the microwave signal in Fig. 1 can be explained by a decrease in the plasma density during the REB pulse. It is known [9] that the PRMA gain factor rapidly decreases as the plasma density decreases below its optimal value and decreases more slowly as the plasma density increases above its optimal value. Therefore, one may expect different dependences of the amplitude of the microwave electric field during the REB pulse for different values of the initial plasma density. If we assume that the initial plasma density of 9 rel. units is lower or slightly higher than its optimal value, then the decrease in the plasma density during the REB pulse should lead to fast disruption of amplification. It is this disruption that is observed in Fig. 1a. If we assume that the initial plasma density of 11.5 rel. units significantly exceeds the optimal value, then the decrease in the plasma density during the REB pulse should lead to an increase in the amplitude and duration of the microwave signal, as is observed in Fig. 1c.

Information on the time evolution of the plasma density during the REB pulse can be obtained by recording the emission spectra and analyzing the frequency shift of the output signal relative to the input frequency. The spectra of the PRMA output signals for different values of the plasma electron density are shown in Fig. 2. It is seen that the peaks of the spectra of the amplified signals lie at frequencies below 2.71 GHz and the spectra are wider than the magnetron radiation spectrum. The observed frequency shift can be caused, e.g., by a change in the wave phase velocity in plasma due to the change in the electron density during the microwave pulse. This leads to a change in the phase increment along the length of the plasma column, which manifests itself as variation in the frequency the PRMA output signal. Note that, in a plasma microwave oscillator, the mechanism of variation in the signal frequency with varying plasma density is different: in this case, conditions for the resonance excitation of an electromagnetic wave by the electron beam change. This leads to a more significant shift in the output frequency of the microwave oscillator [10, 11].

Analysis of the spectra in different time intervals shows that the radiation frequency as a whole decreases with time. A more detailed time dependence of the radiation frequency is obtained by measuring the duration of different periods of the microwave signal. The results of such measurements are presented in Fig. 3, where curves *1–3* correspond to signals shown in Figs. 1a–1c, respectively. At a low plasma density (curve *1*), the amplified signal is present only in the beginning of the REB pulse, up to the time $t = 350$ ns. In this case, the signal frequency is below the frequency of the magnetron by about 10 MHz. At a high plasma density (curve *3*), the first part of the pulse contains a weak harmonic signal and significant REB

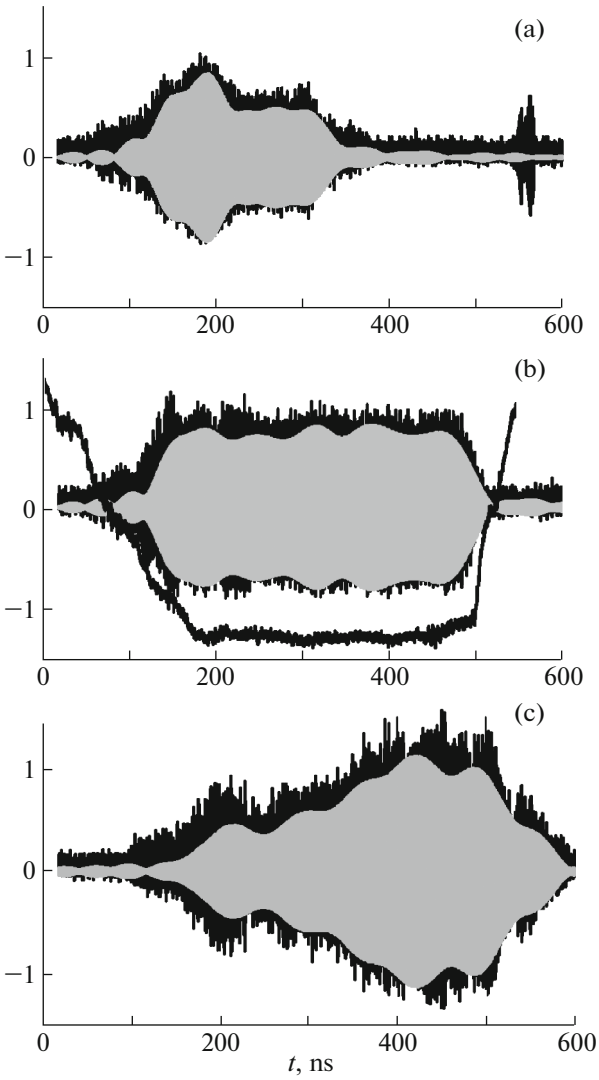

Fig. 1. Waveforms of the microwave signal at the output of the PRMA: the measured signal (black) and the signal processed by a ±15-MHz bandpass filter in the vicinity of 2.71 GHz (gray). The plasma density and the maximum pulse power are (a) 9 rel. units and 50 MW, (b) 9.9 rel. units and 70 MW, and (c) 11.5 rel. units and 130 MW, respectively. Panel (b) also shows the waveform of the voltage at the accelerator cathode.

noise, while in the second part, the amplified harmonic signal at a frequency close to $f = 2.71$ GHz is dominating. It should be noted that the magnetron signal in the absence of an REB pulse has a stable frequency of $f = 2.71$ GHz during the entire observation time.

Thus, the experimental results demonstrate instability of the frequency of the PRMA output signal. Generally, we observe a reduction in the output frequency relative to the input frequency. This instability cannot be explained by the instability of the magnetron used as the source of the input signal. The variability of the directed velocity of the REB electrons due to the unsteadiness of the accelerating voltage also does not provide the observed frequency shift of the PRMA output signal by a few megahertz. Apparently, the main factor resulting in the PRMA instability is the unsteadiness of the density of the tubular plasma. This unsteadiness cannot be explained by the ordinary decay of the plasma prepared before REB injection. It was established experimentally that this plasma decayed over a time longer than 100 μs. Although some plasma electrons escape onto the wall due to the electrostatic field of the electron beam, the corresponding decrease in the plasma electron density is insignificant—on the order of the REB density. Another mechanism for the plasma decay that can lead to a substantial fast decrease in the electron density is their escape onto the wall along the magnetic field due to a significant increase in their mean energy in the high-power microwave field and the appearance of accelerated electrons in plasma [12]. Additional gas ionization in the strong microwave fields does not occur, because the initially prepared plasma is almost fully ionized.

3. INTERPRETATION OF EXPERIMENTAL RESULTS

For the given PRMA geometry, the linear dispersion relation can be obtained by matching the solutions to the wave equation in the domains $0 < r < r_b$, $r_b < r < r_p$, and $r_p < r < R$ with allowance for the boundedness of the solution at $r = 0$ and the vanishing of the tangential component of the electric field at the metal surface ($r = R$) [9]. Here, r_b and r_p are the mean radii of the electron beam and the plasma, respectively, and R is the radius of the cylindrical waveguide. For simplicity, we use the approximation of infinitely thin beams and plasma, i.e., the thicknesses of the walls of the plasma column and annular electron beam (Δ_p and Δ_b, respectively) are assumed to be much smaller than the other characteristic dimensions. The entire system is placed in a strong external magnetic field, which magnetizes both the beam electrons and the plasma. The dispersion relation that gives the complex wavenumber of the excited axisymmetric wave as a function of the signal frequency at the input of the electrodynamic system has the form [9]

$$\left(\omega^2 - \omega_p^2 \frac{\chi^2}{k_{\perp p}^2}\right)\left((\omega - k_z u)^2 - \omega_b^2 \gamma^{-3} \frac{\chi^2}{k_{\perp b}^2}\right) = \Theta \omega_p^2 \frac{\chi^2}{k_{\perp p}^2} \omega_b^2 \gamma^{-3} \frac{\chi^2}{k_{\perp b}^2}, \quad (1)$$

where $\chi^2 = k_z^2 - \omega^2/c^2$;

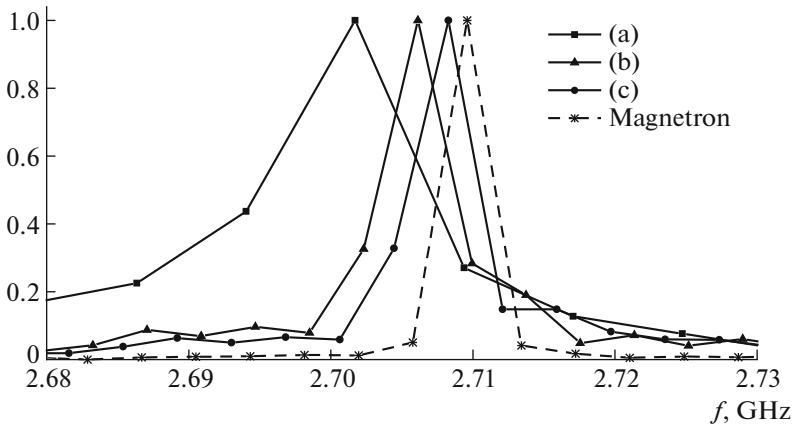

Fig. 2. Spectra of the microwave signals shown in Figs. 1a–1c and the spectrum of the magnetron signal. The spectrum of signal (a) was calculated over a time interval of 200–330 ns, while the other spectra were calculated over a time interval of 200–462 ns.

$$k_{\perp p,b}^2 = \left\{ r_{p,b}\Delta_{p,b} I_0^2(\chi r_{p,b}) \left[\frac{K_0(\chi r_{p,b})}{I_0(\chi r_{p,b})} - \frac{K_0(\chi R)}{I_0(\chi R)} \right] \right\}^{-1}; \quad (2)$$

$$\Theta = \frac{I_0(\chi r_b)}{I_0(\chi r_p)} \frac{K_0(\chi r_p) I_0(\chi R) - K_0(\chi R) I_0(\chi r_p)}{K_0(\chi r_b) I_0(\chi R) - K_0(\chi R) I_0(\chi r_b)}; \quad (3)$$

and $I_0(x)$ and $K_0(x)$ are the zero-order modified Bessel functions of the first and second kinds, respectively. A more general case of electromagnetic interaction between an electron beam and plasma with allowance for the finiteness of the guiding magnetic field was considered in [13, 14].

Under the Cherenkov beam–plasma interaction, waves with phase velocities close to the beam velocity u are amplified; therefore, the solution to Eq. (1) is sought for in the form

$$k_z = \frac{\omega}{u}(1+\delta), \quad (4)$$

where $|\delta| \ll 1$. The imaginary part δ determines the dimensionless spatial amplification coefficient, while its real part describes the excess of the beam velocity over the phase velocity of the amplified wave. Substituting expression (4) into dispersion relation (1), we reduce it to the cubic equation

$$\left[1 - \alpha_p\left(1 + 2\gamma^2\delta\right)\right]\left[\delta^2 - \alpha_b\left(1 + 2\gamma^2\delta\right)\right] = \Theta\alpha_p\alpha_b\left(1 + 2\gamma^2\delta\right)^2, \quad (5)$$

where

$$\alpha_p = \frac{\omega_p^2}{k_{\perp p}^2 u^2 \gamma^2}, \quad \alpha_b = \frac{\omega_b^2 \gamma^{-3}}{k_{\perp b}^2 u^2 \gamma^2} \quad (6)$$

and expressions (2), (3), and (6) are taken at $k_z = \omega/u$. The vanishing of the first factor in Eqs. (5) and (1) determines the spectrum of the surface plasma wave, $k_z(\omega)$. Equating the second factor in Eqs. (5) and (1) to zero gives the spectrum of the beam waves, $k_z(\omega)$. The coupling of the plasma and beam subsystems through the right-hand sides of Eqs. (1) and (5)) results in the wave amplification, i.e., the wavenumber k_z and quantity δ acquire imaginary parts. Equation (5) can easily be solved with respect to the unknown δ. The results of the solution (the real and imaginary parts of δ as functions of the plasma electron density) are presented in Fig. 4. The calculations were performed for the electron beam velocity of $u = 2.6\times10^{10}$ cm/s, waveguide radius of $R = 4.9$ cm, of $r_p = 2$ cm, mean beam radius of $r_b = 1.25$ cm, plasma wall thickness of $\Delta_p = 0.2$ cm, and beam wall thickness of $\Delta_b = 0.5$ cm. These values correspond to the parameters of the beam–plasma system in the experiment described above. At a low plasma electron density $n_p < 0.76\times10^{12}$ cm^{-3}, there is no amplification. The maximum amplification at the frequency of 2.71 GHz for the given parameters is reached at

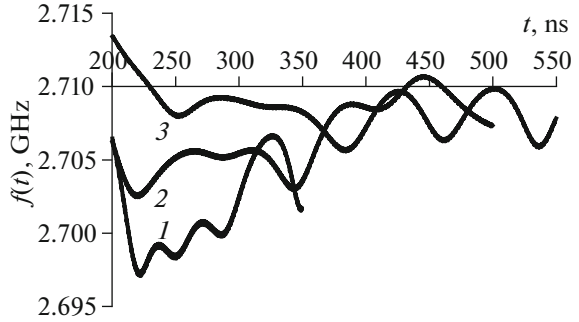

Fig. 3. Time dependences of the frequency of the output signal $f(t)$. Curves *1–3* correspond to Figs. 1a–1c, respectively.

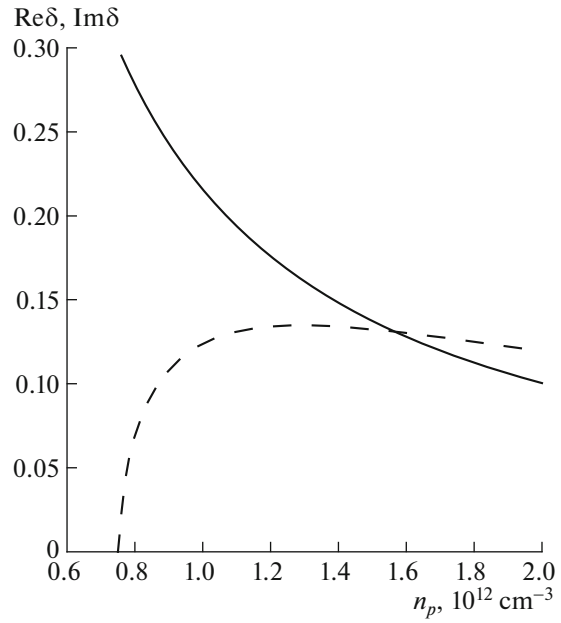

Fig. 4. Real (solid curve) and imaginary (dashed curve) parts of the dimensionless amplification factor δ vs. plasma electron density.

$n_p \approx 1.3\times10^{12}$ cm^{-3}. The behavior of $\mathrm{Im}\,\delta$ as a function of n_p near the optimal value $n_p \approx 1.3\times10^{12}$ cm^{-3} differs significantly as n_p decreases or increases. When the plasma electron density decreases, the amplification factor decreases rather rapidly. When n_p increases, $\mathrm{Im}\,\delta$ decreases much more slowly. The real part $\mathrm{Re}\,\delta$ increases monotonically with n_p in the entire range of the electron density where the amplification of the plasma wave takes place.

Strictly speaking, dispersion relation (5) is obtained under the assumption that all the parameters do not vary in time. If the plasma density $n_p(t)$ is a slowly varying function of time, then dispersion relation (5) is valid and its solution $\delta(t)$ is also a slowly varying function of time. This approach is similar to the geometrical optics approach, and Eq. (5) is an analog of the eikonal equation [15]. The real part $\mathrm{Re}\,k_z(t) = (1 + \mathrm{Re}\,\delta(t))\,\omega/u$ (the wavenumber of the amplified wave) determines the phase increment of the amplified wave as it propagates from the input of the amplifier at $z = 0$ toward its output at $z = L$. Since the phase increment is a slowly varying function of time, the frequency at the amplifier output can differ from the input frequency. Let us find the frequency of the output signal with the phase modulated in time. At the time point t, the wave phase at $z = L$ is

$$\varphi(t) = \omega t - \mathrm{Re}\,k_z(t)\,L. \tag{7}$$

During one wave period T, the phase increases by 2π, i.e.,

$$\begin{aligned}&\varphi(t+T) - \varphi(t)\\ &= \omega T - (\mathrm{Re}\,k_z(t+T) - \mathrm{Re}\,k_z(t))\,L = 2\pi.\end{aligned} \tag{8}$$

Introducing the circular frequency $\omega(t) = 2\pi/T$ and taking into account that $k_z(t)$ is a slowly varying function of time, we obtain

$$\begin{aligned}&\omega(t) = \omega - L\frac{d\,\mathrm{Re}\,k_z(t)}{dt} = \omega\left(1 - \frac{L}{u}\frac{d\,\mathrm{Re}\,\delta(t)}{dt}\right),\\ &\text{or}\quad f(t) = f\left(1 - \frac{L}{u}\frac{d\,\mathrm{Re}\,\delta(t)}{dt}\right).\end{aligned} \tag{9}$$

Relationship (9) shows that the difference between the output and input frequencies, $\Delta f(t) = f(t) - f$, is determined by the derivative $dn_p(t)/dt$. If the plasma density is independent of time, then the amplified signal has the same frequency f as the input signal.

The value of $d\,\mathrm{Re}\,\delta(t)/dt$ found from expression (9) allows us to determine $n_p(t)$. Indeed, solving dispersion relation (5), we find the dependences $\delta(n_p)$. From the dependence corresponding to the amplified wave, we obtain

$$\frac{d\,\mathrm{Re}\,\delta}{dt} = \left.\frac{d\,\mathrm{Re}\,\delta}{dn_p}\right|_{\mathrm{Im}\,\delta<0}\frac{dn_p}{dt}. \tag{10}$$

For convenience, we introduce the dimensionless plasma electron density $\tilde{n}_p = n_p/n_{p0}$, where $n_{p0} = 10^{12}$ cm^{-3} is the characteristic value of the electron density in the problem under study. Dividing the right- and left-hand sides of relationship (10) by $\tilde{n}_p^{2.2}$, we rewrite it in the form

$$\frac{d\tilde{n}_p^{-1.2}/dt}{d\,\mathrm{Re}\,\delta/dt} = -1.2\left(\tilde{n}_p^{2.2}\left.\frac{d\,\mathrm{Re}\,\delta}{d\tilde{n}_p}\right|_{\mathrm{Im}\,\delta<0}\right)^{-1}. \tag{11}$$

This choice of such a transformation is due to the fact that the right-hand side of Eq. (11) in the range of electron densities of interest to us is practically independent of $\tilde{n}_p$. As the plasma density varies from 0.8×10^{12} to 2×10^{12} cm^{-3}, the right-hand side of Eq. (11) remains equal to $\gamma = 4.9$. This allows us to approximately solve Eq. (11) and find the sought-for dependence $n_p(t)$. From Eqs. (9) and (11), we obtain

$$\tilde{n}_p^{-1.2}(t) = \tilde{n}_p^{-1.2}(t_0) + \xi, \tag{12}$$

where the quantity

$$\xi = -\frac{\gamma u}{fL}\int_{t_0}^{t}\Delta f(t)\,dt \tag{13}$$

characterizes variation in the plasma electron density. Integration in formula (13) is performed from the

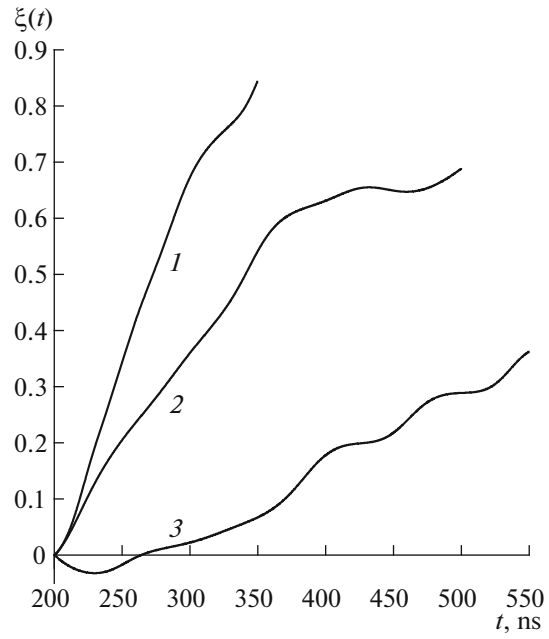

Fig. 5. Dependences $\xi(t)$ for three curves *1–3* shown in Fig. 3.

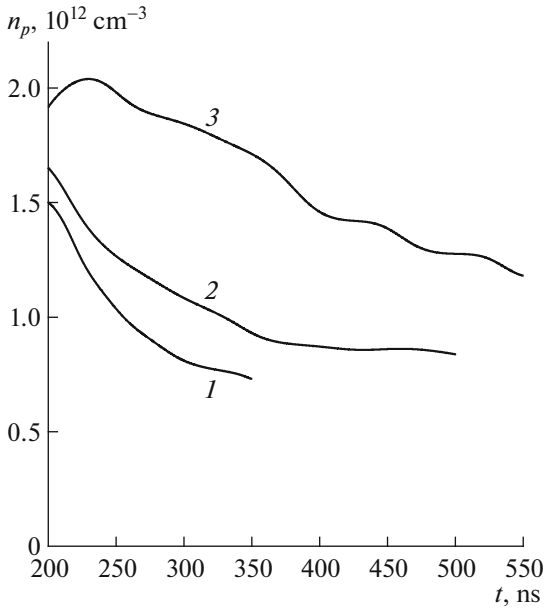

Fig. 6. Time dependences of the plasma electron density for three curves *1–3* shown in Fig. 3.

time t_0 at which the plasma electron density $\tilde{n}_p(t_0)$ is known. The difficulty in determining the dynamics of the electron density is that we know only the relative electron density and only at the time of its creation. However, the electron energy in the REB pulse reaches its steady-state level only at the time t_0 = 200 ns (Fig. 1b). Therefore, we will assume that, at this time, the plasma electron densities corresponding to Figs 1a–1c are 1.5×10^{12}, 1.65×10^{12}, and 1.92×10^{12} cm^{-3}, respectively. The length of the plasma column in the experiment is L = 50–70 cm. The dependences $\xi(t)$ corresponding to three curves in Fig. 3 are shown in Fig. 5.

The, using formula (12), we can find the time evolution of the plasma electron density during the microwave pulse (see Fig. 6). In all cases, the plasma density decreases significantly during the REB pulse.

Assuming that the amplification processes are linear, we find that the ratio between the amplitudes of the output and input signals is given by the formula

$$\frac{E_{\text{out}}}{E_{\text{in}}} = \exp\left(\frac{\omega}{u}\operatorname{Im}\delta L\right) \qquad (14)$$

and, for the given values of the parameters, is on the order of 10^2. Comparing this value with the experimentally determined power amplification factor 2×10^3, we can conclude that, in this case, an almost linear amplification regime with saturation near the amplifier output is implemented. Figure 7 shows the time dependences calculated by formula (14) for three time profiles $n_p(t)$ shown in Fig. 6. In general, these dependences agree qualitatively with the waveforms shown in Fig. 1. For a low initial plasma electron density, amplification is disrupted at t = 300 ns. No disruption of amplification is observed for larger values of the initial plasma density; in this case, the signal amplitude can either decrease or increase with time.

4. NUMERICAL SIMULATION OF REB–PLASMA INTERACTION

In the previous sections, the process of amplification of the input microwave signal by a PRMA was studied experimentally and analytically under the assumption that the plasma density gradually decreases in time. Numerical simulations can provide information on both the process of plasma wave amplification and the time evolution of the parameters of beam–plasma interaction during the REB pulse, such as the plasma density, mean energy of plasma electrons, and plasma potential. In the previous numerical simulations of a PRMA, the plasma parameters were assumed invariable during the REB pulse and the plasma was described in the linear approximation [16]. In the present work, numerical simulations were performed using the KARAT particle-in-cell (PIC) code [17, 18], which allows one to self-consistently take into account time variations in the plasma parameters. The full system of Maxwell's equations was solved. Of course, the model cannot take into account all factors present in an actual experiment. We successively complemented the model with new ele-

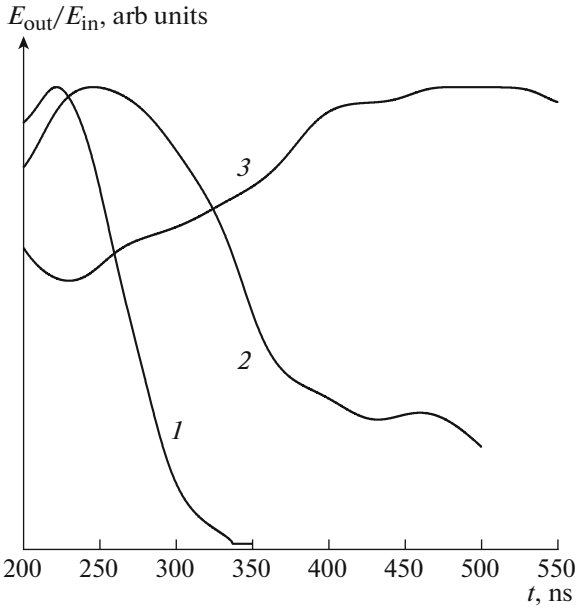

Fig. 7. Time dependence of the amplitude of the microwave signal at the output of the amplifier for three curves *1–3* shown in Fig. 6.

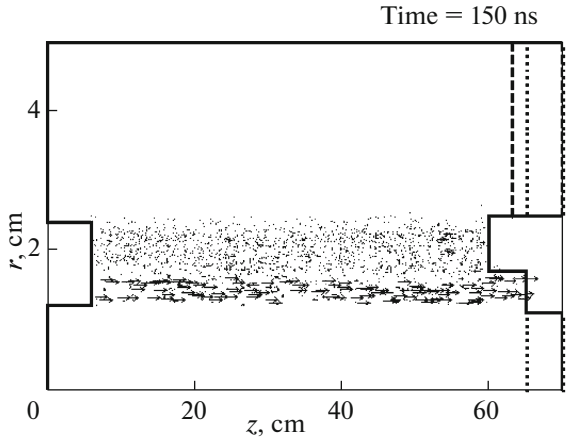

Fig. 8. Geometry of the numerical model.

ments. First, we used an axisymmetric model, in which the simulation was restricted to the region of interaction of the beam with the plasma and the amplified wave. The asymmetric horn for radiation output, the asymmetric absorbing elements located at the periphery of the beam–plasma interaction region, the electron beam formation region, and the system for input of radiation from an external microwave source were not considered. The time dependences of the energy of beam electrons and the beam current and the geometry of the region of interaction between the electron beam and the electromagnetic wave were taken from the experiment. The plasma density before REB injection into the system in relative units also was known from the experimental data. Absolute measurements of the plasma density in the experiment were not performed. In order to improve the simulation accuracy, the wall thickness of the tubular plasma was increased in the simulations by a factor of 3 compared to its actual value. According to analytical theory, the wall thickness of the tubular plasma insignificantly affects the process of amplification of the plasma microwave. In accordance with the increased wall thickness of the tubular plasma, the initial plasma electron density was reduced in comparison with that used above and was set in the simulations at 0.75×10^{12} cm^{-3}. The initial plasma temperature was assumed to be 5 eV. Variations in the initial temperature from 0 to 10 eV do not affect the simulation results. Ionization processes were not considered.

Figure 8 shows the computational domain in the (r, z) geometry. We used a rectangular mesh, in most cases, with 100 nodes over r and 1400 nodes over z. The solid line shows the grounded conductive surface on the left and on top and also the metal collector on the right at $r < 2.5$ cm. In the experiment, the collector was grounded and the system for radiation output was well matched and almost transparent for microwave radiation. In the numerical model, the collector was grounded through a circuit with a dominantly inductive impedance coinciding with the experimental one. Since the vacuum coaxial line admits other types of waves, to suppress their reflection, the model was complemented with a region absorbing electromagnetic radiation (z = 65–70 cm), which is bounded by the dashed line. The model plasma particles are represented by points in the region 1.6 cm $< r <$ 2.2 cm, and the arrows below represent the beam electrons injected from the left. The current increases linearly from 25 to 180 ns and reaches 2 kA, while the electron energy in the same time interval varies from 70 to 500 keV, which agrees with the experiment (see Fig. 1b)

The process of plasma formation is not simulated. At the initial time, in the given region, there are cold singly ionized Xe ions and electrons with a density of 0.75×10^{12} cm^{-3}. The electrons have a Maxwellian distribution with an initial temperature of 5 eV. The total number of model particles in the simulations was on the order of 10^6, which corresponded to more than 10 model particles per cell occupied by the beam or plasma.

The maximum value of the magnetic field was 4.5 kG, and the magnetic field profile corresponded to the experimental one. The energy of beam electrons was modulated at a frequency of 2.71 GHz with an amplitude of 3%, which modeled in a simplified manner the signal from the magnetron in the actual amplifier.

Let us consider some results of simulations in the given formulation. In the experiment, the fields at the output of the horn are measured, but the horn is not

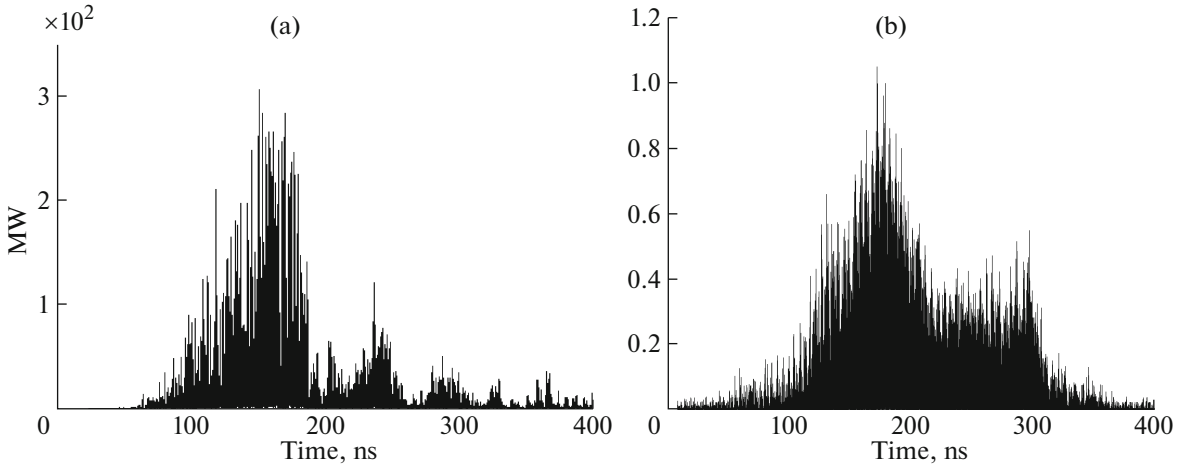

Fig. 9. Time dependences of the (a) calculated radiation power for a plasma density of 0.75×10^{12} cm^{-3} and (b) measured radiation power (in rel. units) corresponding to Fig. 1a.

included in the computational model; therefore, the time dependence of the flux of the Poynting vector through the cross section in front of the absorber in the vacuum coaxial waveguide at $z = 65$ cm was chosen as an analog of the experimental data (Fig. 9a). Note that the maximum power is close to that given in the caption of Fig. 1. It can be seen that the radiation power is maximal between 130 to 200 ns, after which it decreases. The experimental time dependence of the squared amplitude of the signal shown in Fig. 1a is shown in Fig. 9b. This dependence almost coincides with the calculated one. In the simulations, a decrease in the frequency of output radiation during the microwave pulse was detected. In the time interval of 100–150 ns, the radiation frequency coincides with the input signal frequency of 2.71 GHz, whereas in the time interval of 250–300 ns, the frequency has passed to the adjacent harmonic of the discrete Fourier spectrum (from 2.71 to 2.69 GHz).

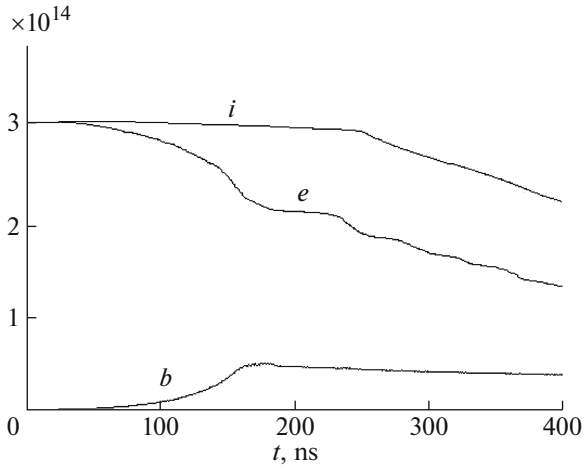

Fig. 10. Time dependence of the total number of particles: (*i*) ions, (*e*) plasma electrons, and (*b*) beam electrons.

Thus, for the given plasma density, the radiation parameters turned out to be close to the experimental ones. An increase in the initial plasma density did not lead to an increase in the pulse duration.

Let us now consider time variations in the plasma parameters during REB injection, i.e., the processes that have not been studied experimentally or analytically. Figure 10 shows the time dependence of the total number of particles. The total number of plasma electrons decreases for 400 ns by a factor of 2.3, while the experimentally measured decay time of a preliminary prepared plasma in the absence of an REB exceeds 100 μs. The reason for such a rapid plasma decay is the sharp increase in the mean energy of plasma electrons (see Fig. 11). It follows from Fig. 11a that the wall thickness of the tubular plasma does not change, because electrons are strongly magnetized. However, the maximum plasma density decreases by a factor of 2, which is close to the decrease in the total number of plasma electrons, which is reduced by a factor of 2.3. The reason for this is the sharp increase in the kinetic energy of electrons (the mean value is about 30 keV, see Fig. 11b). Such a high mean energy of plasma electrons leads to their rapid escape along the magnetic field (along z axis) and the appearance of a high positive plasma potential of about 150 kV (see Fig. 12).

Such a large discrepancy between the mean kinetic energy of plasma electrons and plasma potential indicates that the plasma is nonequilibrium and there are a large number of electrons with energies significantly exceeding the mean electron energy. Separate electrons with energies of up to 150 keV were detected.

Figure 13 shows the dynamics of ions. Since the ions are not magnetized, they expand both along and

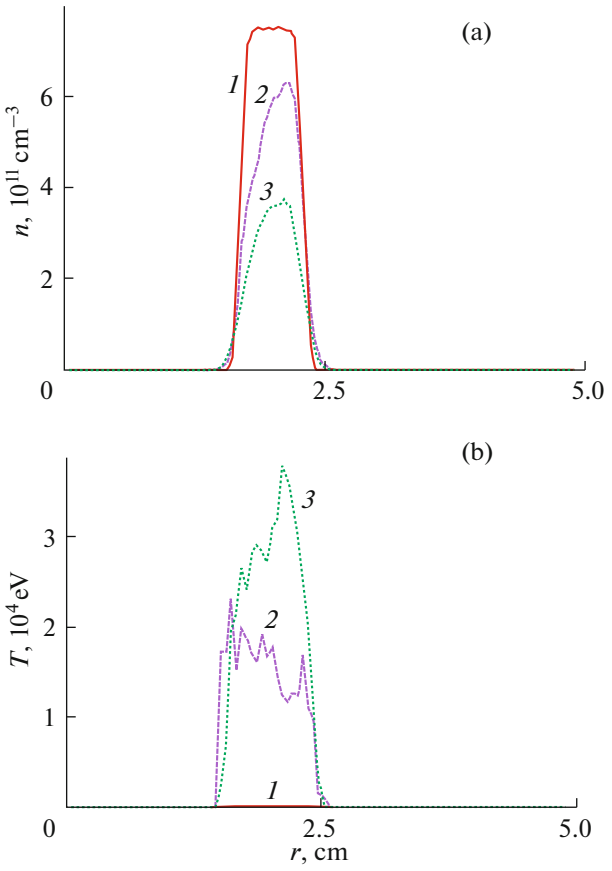

Fig. 11. (Color online) Radial profiles of the (a) density and (b) mean kinetic energy of plasma electrons for three instants of time: (*1*) 0, (*2*) 150, and (*3*) 300 ns at $z = 35$ cm.

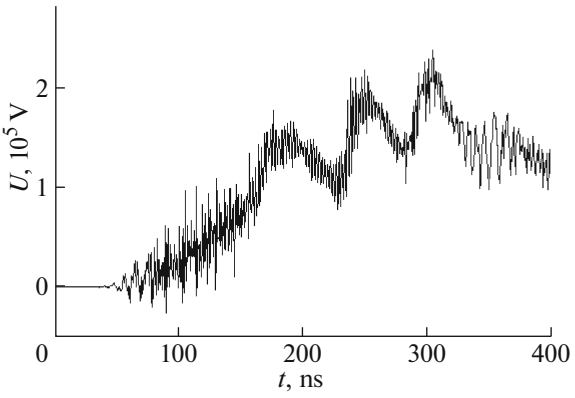

Fig. 12. Time dependence of the electric potential in the tubular plasma at $r = 1.9$ and $z = 35$ cm.

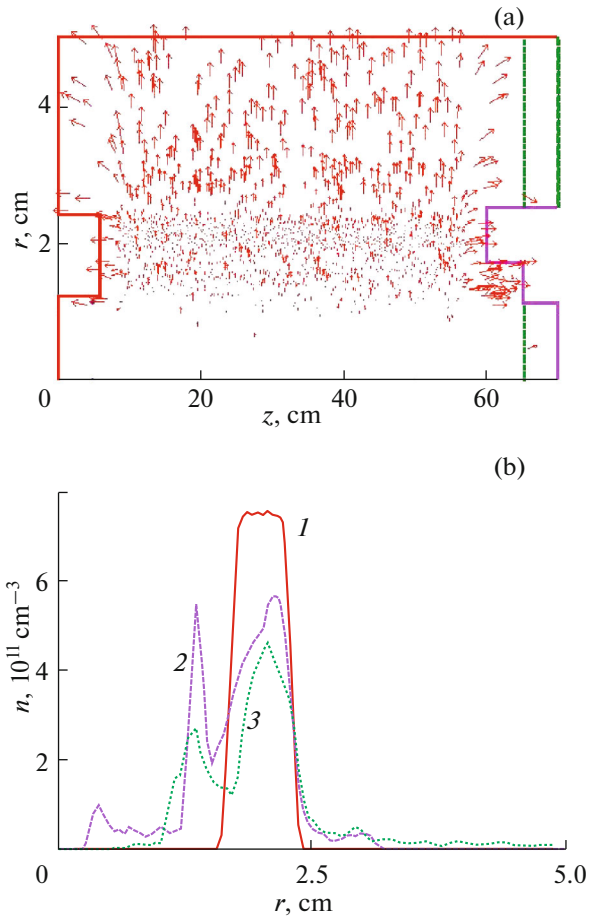

Fig. 13. (Color online) (a) Ion velocity field at $t = 300$ ns and (b) radial profiles of the ion density at $z = 35$ cm at times (*1*) 0, (*2*) 150, and (*3*) 300 ns.

across the axis due to the presence of a positive potential in the plasma region. In this case, they acquire an energy of up to 150 keV. It should be noted that the increase in the rate of decrease in the number of ions at the time of 250 ns (see Fig. 10) coincides with the time at which ions reach the side wall of the vacuum chamber. It follows from Fig. 13b that the ion density in the region $r > 2.5$ cm is low and a significant fraction of ions are in the region occupied by the electron beam, thereby neutralizing its charge.

The behavior of the system illustrated in Figs. 10–13 can be qualitatively described as follows. Due to the amplification of the electromagnetic wave in the beam–plasma system, the kinetic energy of plasma electrons significantly increases and electrons escape along the magnetic field onto the chamber ends. This leads to an increase in the plasma potential. Starting from the time of 250 ns, a balance of several processes is established: escape of ions onto the chamber walls; escape of electrons onto the chamber ends; excitation of the electronic subsystem, due to which separate electrons acquire energies of about 150 keV, which is sufficient to overcome the potential barrier; and the resulting stabilization of the plasma potential.

Thus, within the above-formulated problem of finding reasons for the dependence of the frequency and shape of the microwave pulse in a PRMA on the initial plasma density, the most important result of

numerical simulation is the discovery of rapid plasma decay. In the numerical simulations, the plasma density decreases nearly by a factor of 2 for 300 ns, whereas from analysis of the experimental data presented in Fig. 1a, it was found that the plasma density should decrease by a factor of 2 for 150 ns. Taking into account all adopted approximations, the results of both models may be considered close to one another.

In the analytical calculation, it was assumed that the electron energy was 500 keV. The computer simulations demonstrate that the energy of beam electron is 665–680 keV after 180 ns. Such a change in the energy of a relativistic beam leads to a relatively small (about 3%) increase in the electron velocity and does not affect the results obtained in Section 3. Escape of ions from the plasma channel also has little effect on the dynamics of beam–plasma instability, because, due to the large ion mass, the decisive contribution to the interaction with the electromagnetic wave in the microwave frequency range is made by the electron component.

5. CONCLUSIONS

The dependence of the shape of the microwave pulse in a PRMA on the initial plasma electron density in the system has been detected experimentally. Depending on the plasma density, fast disruption of amplification, stable operation of the amplifier during the REB pulse, and its delayed actuation can take place. A reduction in the frequency of the output signal relative to the magnetron frequency was observed experimentally. The change in the shape of the microwave signal and the reduction in its frequency are explained by a reduction in the plasma density in the PRMA. A change in the plasma density leads to a change in the phase velocity of the amplified wave, which results a time-dependent increment of the wave phase at the output of the plasma waveguide and a shift in the radiation frequency. Different shapes of the PRMA output signal are determined by a change in the amplification factor, which, in turn, is caused by a reduction in the plasma electron density. Using the linear theory of amplification in a PRMA with a thin-wall hollow electron beam and plasma, the dynamics of the plasma density during the REB pulse is qualitatively determined from the experimental data. The experimental and theoretical studies have been supplemented by direct numerical simulations of the processes in a PRMA. In the numerical simulations, information on the process of amplification of the plasma wave and the time evolution of the parameters of beam–plasma interaction during the REB pulse has been obtained. It is shown that, during the REB puls, the mean energy of plasma electrons increases, while the electron density decreases significantly. The analytical results and numerical simulations satisfactorily agree with the experimental data and allow one to explain the observed frequency shift of the amplified signal.

ACKNOWLEDGMENTS

This work was supported in part by the Russian Foundation for Basic Research, project no. 16-08-00439.

REFERENCES

1. R. J. Barker and E. Schamiloglu, *High-Power Microwave Sources and Technologies* (IEEE Press, New York, 2001).
2. *Proceedings of the International Workshop on High-Power Microwave Generation and Pulse Shortening, Edinburgh, 1997.*
3. F. S. El'chaninov, F. Ya. Zagulov, S. D. Korovin, G. A. Mesyats, and V. V. Rostov, Sov. Tech. Phys. Lett. **6**, 500 (1981).
4. O. T. Loza, P. S. Strelkov, and S. N. Voronkov, Plasma Phys. Rep. **20**, 617 (1994).
5. N. F. Kovalev, V. E. Nechaev, M. I. Petelin, and N. I. Zaitsev, IEEE Trans. Plasma Sci. **26**, 246 (1998).
6. P. S. Strelkov, V. P. Tarakanov, I. E. Ivanov, and D. V. Shumeiko, Plasma Phys. Rep. **40**, 640 (2014).
7. P. S. Strelkov, V. P. Tarakanov, I. E. Ivanov, and D. V. Shumeiko, Plasma Phys. Rep. **41**, 492 (2015).
8. O. T. Loza, A. V. Ponomarev, D. K. Ul'yanov, P. S. Strelkov, and A. G. Shkvarunets, Plasma Phys. Rep. **23**, 201 (1997).
9. M. V. Kuzelev, A. A. Rukhadze, and P. S. Strelkov, *Plasma Relativistic Microwave Electronics* (Mosk. Gos. Tekhn. Univ. im. N.E. Baumana, Moscow, 2002) [in Russian].
10. D. K. Ul'yanov, R. V. Baranov, O. T. Loza, S. E. Ernyleva, and I. L. Bogdankevich, Tech. Phys. **58**, 1503 (2013).
11. O. T. Loza, D. K. Ul'yanov, and R. V. Baranov, Tech. Phys. **56**, 413 (2011).
12. V. P. Tarakanov and E. G. Shustin, Plasma Phys. Rep. **33**, 130 (2007).
13. I. N. Kartashov, M. V. Kuzelev, and A. A. Rukhadze, Plasma Phys. Rep. **30**, 56 (2004).
14. I. N. Kartashov, M. V. Kuzelev, and A. A. Rukhadze, Plasma Phys. Rep. **35**, 169 (2009).
15. A. A. Rukhadze and V. P. Silin, Sov. Phys. Usp. **7**, 209 (1964).
16. I. L. Bogdankevich, I. E. Ivanov, and P. S. Strelkov, Plasma Phys. Rep. **36**, 762 (2010).
17. V. P. Tarakanov, *Mathematical Modeling: Problems and Results* (Nauka, Moscow, 2003) [in Russian].
18. V. P. Tarakanov, *User's Manual for Code KARAT* (Berkley Research Associates, Springfield, VA, 1992).

Translated by E. Chernokozhin